k-space-resolved inverse-photoemission study of ZrC(100) and VC(100)

K. L. Håkansson, H. I. P. Johansson, and L. I. Johansson
Department of Physics and Measurement Technology, Linköping University, S-581 83 Linköping, Sweden
(Received 29 December 1992)

A *k*-space-resolved inverse-photoemission study of ZrC(100) and VC(100) along the ⟨010⟩ and ⟨011⟩ azimuthal directions for emitted photons of 9.8 eV is presented. Recorded spectra are compared with theoretical spectra calculated using the time-reversed low-energy-electron-diffraction scheme. The calculated spectra are shown to reproduce the relative intensities and the trends in the peak dispersions fairly well. However, when probing states along the Δ direction, only final states of Δ_5 symmetry are observed experimentally, although transitions to Δ_1 states are also predicted in the calculation.

I. INTRODUCTION

The occupied valence bands of ZrC(100) (Refs. 1–3) and VC(100) (Refs. 4–7) have been investigated earlier using angle-resolved photoelectron spectroscopy (ARPES), both utilizing conventional discharge lamps and synchrotron radiation. High-resolution core-level studies of those two transition-metal carbides have also been presented recently.[8,9] No experimental study of the unoccupied valence bands of these two carbides has, however, been reported and therefore we have used *k*-space-resolved inverse photoelectron spectroscopy[10,11] to study the unoccupied band structure above the Fermi level.

In this paper a study of the unoccupied electronic structure of $ZrC_{0.92}(100)$ and $VC_{0.80}(100)$ single crystals is presented. *k*-space-resolved inverse photoelectron spectra recorded in the isochromat mode[10] along the ⟨010⟩ and ⟨011⟩ azimuthal directions are presented. The experimental results are compared to theoretical spectra, calculated using the computational scheme originally developed to treat pure ordered metals[12] and later developed to include ordered binary compounds.[13] Relative intensities of spectral features as well as locations and dispersions of bands observed experimentally are compared below with calculated results.

II. EXPERIMENTAL AND COMPUTATIONAL DETAILS

A. Experiment

The experimental arrangement consists of an electron gun with variable kinetic energy and a photon detector with a fixed detector window centered around 9.8 eV. The gun and the detector are mounted in the horizontal plane with an angle of 45° in between them. The surface normal of the sample lies in the horizontal plane and it is possible to rotate the sample around an axis perpendicular to this plane in order to vary the incident angle of the electrons. Both the electron gun and the photon detector have been described in more detail earlier.[14] Efforts to improve the energy resolution of the photon detector have, however, been made.[15]

The samples were mounted with their (100) faces perpendicular to the electron beam axis to within ±1° and the crystals azimuths were oriented by low-energy electron diffraction (LEED). The samples were cleaned *in situ* by repeated flash heatings to temperatures around 1600 °C for ZrC and around 1100 °C for VC. The cleanliness of the surfaces were checked by using ARPES and earlier valence-band results.[1,2,4] No contamination-related features were observed and the surfaces were kept clean by flash heatings every fourth hour. The base pressure in the spectrometer was less than 1×10^{-10} Torr.

In the spectra presented below the energies are referred to the midpoint of the Fermi edge and the incident angle (θ_i) is given relative to the surface normal.

B. Calculated spectra

The extended version[13] of the time-reserved LEED scheme[12] was used to calculate *k*-space-resolved inverse photoemission spectra from the (100) surface of stoichiometric ZrC and VC. The self-consistent muffin-tin potentials generated in previously published linearized augmented-plane-wave band-structure calculations[1,4] were utilized as bulk potentials. Ideal crystal conditions were assumed, i.e., the bulk potential and atomic positions were used in all layers. The surface barrier was positioned immediately outside the muffin-tin sphere of the metal atoms in the surface layer and its height was in both cases determined from the measured work function. Lifetime broadening parameters were chosen to be 2.4 and 0.3 eV for the high-energy and low-energy states, respectively, and 21 reciprocal lattice vectors were included in the computations to ensure convergence. Spectra were calculated for both pure *s*- and *p*-polarized light emission. These were then added together to simulate the experimental condition, detection of unpolarized light. A Fermi-Dirac distribution function was superimposed on the calculated spectra and they were finally convoluted with a Gaussian broadening function to simulate an instrumental energy resolution of 0.8 eV. It should be pointed out that only relative intensities within each spectrum should be compared below since no effort has been made to compare absolute intensities.

0163-1829/93/47(24)/16455(5)/$06.00

III. RESULTS AND DISCUSSION

A. ZrC(100)

Spectra recorded at different electron incidence angles from ZrC(100), along the ⟨010⟩ and ⟨011⟩ azimuthal directions, are shown in Figs. 1(a) and 2(a), respectively. Only one prominent feature, located around 5 eV above the Fermi level, is clearly resolved above the scattered background in both azimuths. The corresponding calculated spectra are shown in Figs. 1(b) and 2(b), respectively. Also, these spectra exhibit one dominating feature located at an energy not far from the value obtained for the experimental feature. At normal incidence, i.e., at $\theta_i = 0°$, only transitions between initial states of Δ_1 symmetry and final states of Δ_1 or Δ_5 symmetry are allowed by symmetry selection rules.[10] The band structure calculated along the Δ direction, i.e., between Γ and X, in the Brillouin zone can be used to determine the transitions from which the dominating feature originate. This is illustrated in Fig. 3 where the calculated Δ_1 and Δ_5 bands, above the Fermi level, along the Γ and X direction of $ZrC_{1.0}$ are shown.[1] Three possible direct transitions with final-state

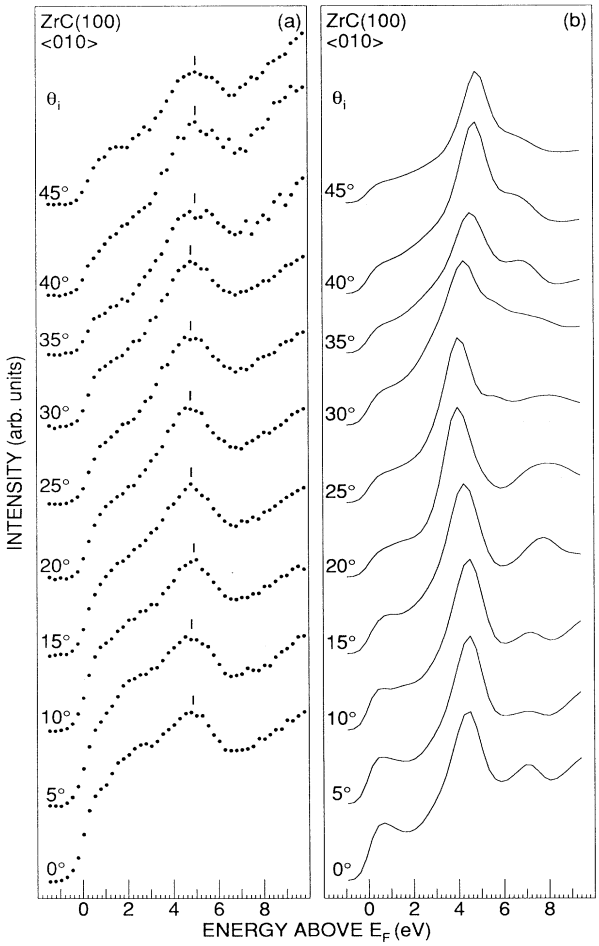

FIG. 1. (a) Experimental and (b) calculated k-space-resolved inverse-photoemission spectra from ZrC(100) along the ⟨010⟩ azimuth at different incident angles θ_i.

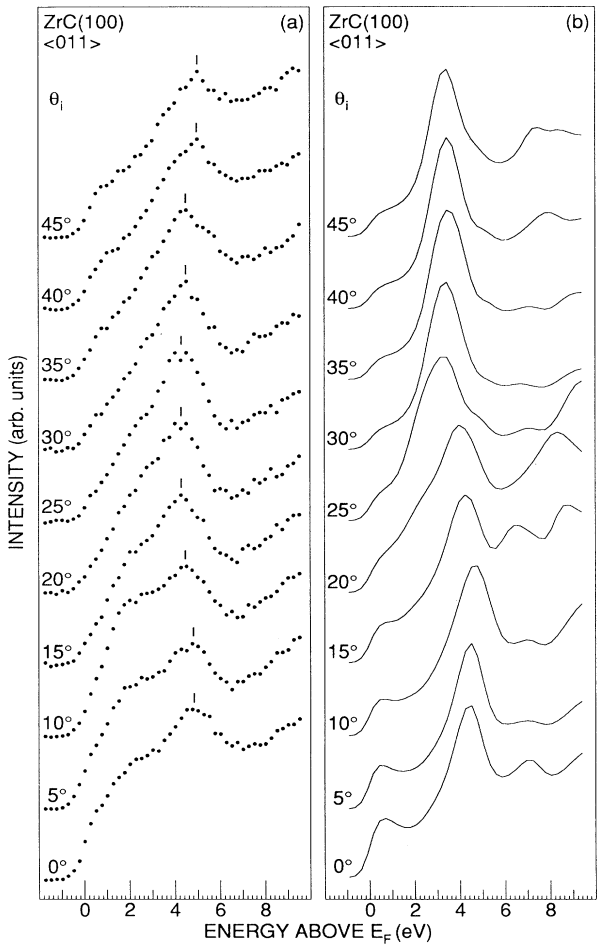

FIG. 2. (a) Experimental and (b) calculated k-space-resolved inverse-photoemission spectra from ZrC(100) along the ⟨011⟩ azimuth at different incident angles θ_i.

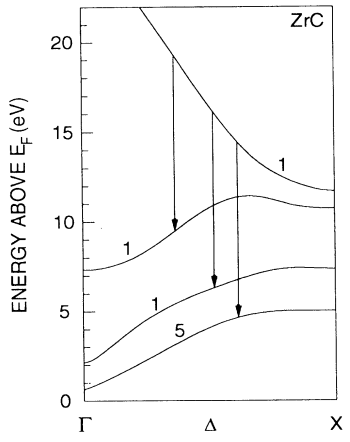

FIG. 3. The Δ_1 and Δ_5 bands along the Γ-X direction for $ZrC_{1.0}$, calculated using the LAPW method. The symmetry-allowed direct transitions, corresponding to photons emitted with an energy of 9.8 eV, are indicated by arrows.

energies below 10 eV above the Fermi level are identified and are indicated by arrows in the figure. Peaks in the calculated normal-incidence spectra corresponding to these transitions can be identified; see Figs. 1(b) and 2(b). The transition to the Δ_5 band give rise to the strong peak located at around 4.5 eV above the Fermi level, the transition to the lowest Δ_1 band give rise to the weaker peak observed around 7 eV, and the transition to the next Δ_1 band give rise to a peak located at around 9.5 eV, which, however, is only partly visible at the end of the spectra shown in Figs. 1(b) and 2(b). Since the calculated results presented in the figures represent the sum of two spectra, one calculated with the polarization vector perpendicular (*s* polarized) and one with the polarization vector parallel (*p* polarized) to the incidence plane, it is possible to identify the symmetry from those spectra. Features in the spectrum calculated with the polarization vector perpendicular to this plane, i.e., parallel to the surface, must arise from final states of Δ_5 symmetry,[10] while with the polarization vector parallel to this plane contribution from final states of both Δ_1 and Δ_5 symmetry are obtained. It is clear from those spectra that the strong feature originates from final states of Δ_5 symmetry while the other two weaker features originate from states of Δ_1 symmetry. Based on these observations the prominent peak located around 5 eV in the experimental normal-incidence spectra is interpreted to originate from transitions to final states of Δ_5 symmetry.

When increasing the incidence angle no strong dispersions of the spectral features are observed. For the ⟨010⟩ azimuth, see Fig. 1, the peak resolved in the experimental spectra show almost no dispersion for incidence angles up to 30°, but at larger incidence angles it moves slightly towards higher energy. The dominant peak in the corresponding calculated spectra exhibits a weak dispersion. During the first 25° it decreases about 0.5 eV in energy whereafter it disperses towards larger energies and finishes at about 0.5 eV larger energy at $\theta_i = 45°$ than at normal incidence. The result for the ⟨011⟩ azimuth is fairly similar; see Fig. 2. In this case, however, the experimentally resolved peak first disperses slightly towards the Fermi level, about 0.5 eV, when increasing the incidence angle to 20°. It is then found to disperse back close to the value obtained at 0° when increasing the angle to 45°. The dominant peak in the calculated spectra along this azimuth first shows a small increase in energy during the first 10°, then it disperses about 1 eV towards the Fermi level when the incidence angle is increased to 25°, whereafter it remains at the same energy up to the largest angle investigated. For ZrC(100) the agreement between experimental and calculated results is quite satisfactory along both azimuthal directions. However, the weaker peaks resolved in the calculated spectra, and identified to originate from final states of Δ_1 symmetry at $\theta_i = 0°$, are not observed in the experimental spectra. This observation will be discussed later, but first we turn to the results for the VC surface.

B. VC(100)

Experimental spectra recorded along the ⟨010⟩ and ⟨011⟩ azimuths from VC(100) are shown in Figs. 4(a) and 5(a), respectively. Two features are clearly resolved in each azimuth, one located around 4–5 eV and strongest at small incidence angles and one located close to the Fermi level which is strongest at large incidence angles. The corresponding calculated spectra are shown in Figs. 4(b) and 5(b), respectively. The difference between experimental and calculated spectra is seen to be somewhat larger in this case. The origin of the feature in the calculated normal-incidence spectra are again possible to determine by utilizing the spectra calculated for the two different polarization directions. The spectrum calculated for *s*-polarized light contains only the peak located around 2 eV and the small feature closest to the Fermi level, while the spectrum calculated for *p*-polarized light also contains the third peak located around 4.5 eV. Using the same arguments as for ZrC(100) the peak around 2 eV thus originates from final states of Δ_5 symmetry while the peak located around 4.5 eV originates from states of Δ_1 symmetry. The corresponding transitions are indicated in Fig. 6 where the calculated Δ_1 and Δ_5 bands, above the Fermi level, along the Γ to X direction of $VC_{1.0}$ are shown.[4] For the transition to the Δ_1 band indicated with a dotted line in Fig. 6 we cannot identify a corre-

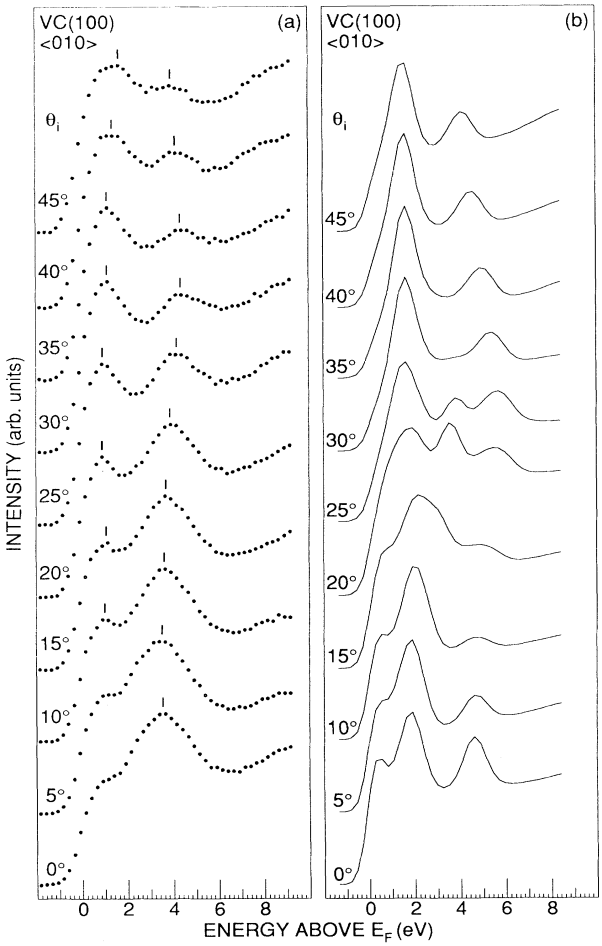

FIG. 4. (a) Experimental and (b) calculated *k*-space-resolved inverse-photoemission spectra from VC(100) along the ⟨010⟩ azimuth at different incident angles θ_i.

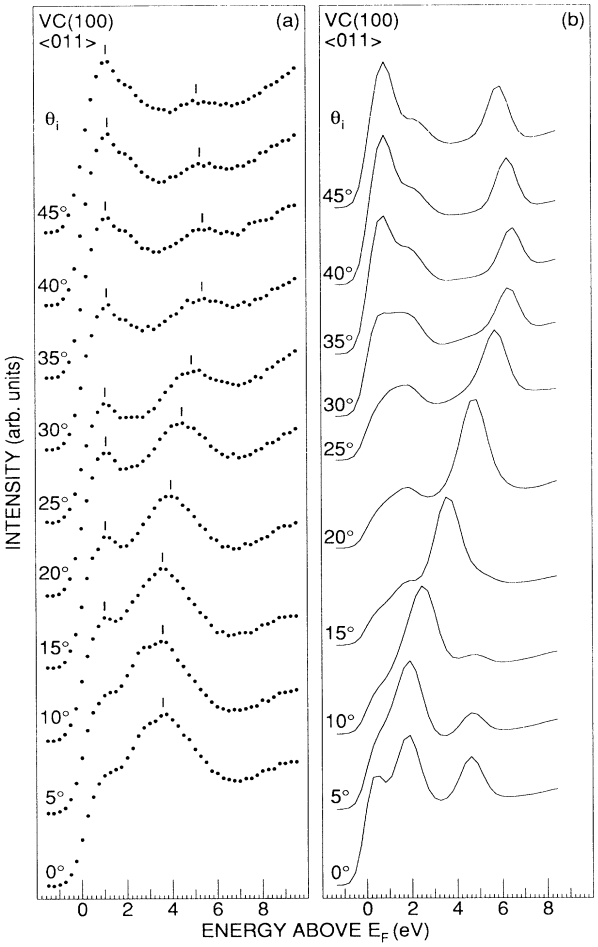

FIG. 5. (a) Experimental and (b) calculated k-space-resolved inverse-photoemission spectra from VC(100) along the ⟨011⟩ azimuth at different incident angles θ_i.

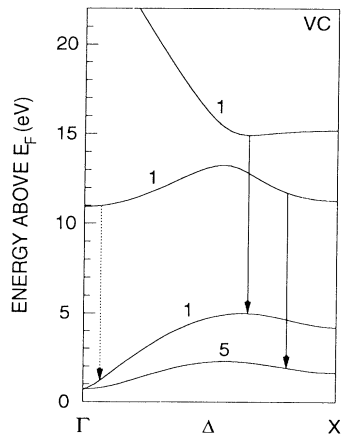

FIG. 6. The Δ_1 and Δ_5 bands along the Γ-X direction for $VC_{1.0}$, calculated using the LAPW method. The symmetry-allowed direct transitions, corresponding to photons emitted with an energy of 9.8 eV, are indicated by arrows.

sponding structure in the calculated spectra. The structure observed closest to the Fermi level in the calculated normal-incidence spectra does not originate from bulk band transitions. It has been pointed out in earlier photoemission calculations[4,7] that the location of this structure depends on the positioning of the surface barrier and that the photocurrent giving rise to this structure is almost entirely localized to the surface layer. This surface-barrier-related feature was found to give the dominant contribution close to the Fermi level in the calculated normal-incidence spectra. In the recorded normal-incidence spectra there is only one well-resolved peak also in this case and the following question arises: To which calculated feature does it correspond? In the case of ZrC(100), only states of Δ_5 symmetry were observed experimentally. The same observation has also been made earlier for TiC(100) and TiN(100).[16] Based on these observations, we interpret the peak, located around 3.5 eV, in the recorded normal-incidence spectra to be of Δ_5 symmetry and to correspond to the peak located around 2 eV above the Fermi level in the calculated spectra. The unoccupied Δ_5 band is thus located about 1.5 eV higher experimentally than theoretically. This is surprising since an earlier photoemission investigation[7] located the occupied Δ_5 band below the Fermi level around 1.5 eV lower experimentally than theoretically. A feature located around 0.5 eV below the Fermi level, exhibiting Δ_5 symmetry, was also observed in these photoemission experiments that did not have a counterpart in the calculated spectra and it was suggested that part of the Δ_5 band located above the Fermi level in the calculations actually might be located below instead.

The largest energy dispersion is found along the ⟨011⟩ azimuth and therefore we start the comparison of experimental and calculated results for the different incident angles along this direction; see Fig. 5. The dominant experimental feature at small incident angles is seen to disperse away from the Fermi level to around 5.5 eV at 35°, whereafter it disperses back slightly towards the Fermi level and decreases in intensity with increasing incidence angle. The peak in the calculated spectra that exhibits a similar behavior is the one located around 2 eV at normal incidence, giving further support to that the experimentally observed peak in the 0° spectrum is of Δ_5 symmetry as suggested above. The energy of this peak first increases with increasing incidence angle up to a maximum energy of about 6.5 eV in the 35° spectrum, whereafter it decreases slightly in energy with increasing angle. The trend in the dispersion of this calculated feature is thus quite similar to that of the experimental peak although the dispersion is considerably larger in the theoretical spectra. The structure located around 1 eV in the experimental spectra which increases in intensity with increasing incidence angle, also has a counterpart in the calculated spectra at the larger angles. A feature develops in the calculated spectra at an angle of about 30° and increases in relative intensity with increasing incidence angle. This feature resembles quite well the behavior observed in the recorded spectra.

Also along the ⟨010⟩ azimuth, see Fig. 4, the experimental spectra show one dispersing structure and one

structure developing close to the Fermi level at the larger incidence angles. The dispersion observed is, however, considerably smaller in this case. The structure located around 3.5 eV at normal incidence is seen to disperse away from the Fermi level to about 4.5 eV when the incidence angle is increased to 30°, whereafter it disperses back slightly and decreases in intensity. The calculated spectra along this azimuth show a different behavior particularly at intermediate angles. The structure located around 2 eV at normal incidence is seen to disperse slightly towards larger energies and to broaden when the angle is increased to 15°. At an angle of 20° the structure has split into two features, one located close to the Fermi level and one located around 3.5 eV, which, moreover, is seen to disperse away from the Fermi level and to decrease in intensity when the angle is increased further. At angles larger than 15° it is thus not possible to identify a structure in the calculated results, shown in Fig. 4, which corresponds to the dispersing structure observed in the recorded spectra. The highest laying structure in the calculated results which at normal incidence originates from a Δ_1 final-state band is not observed at all in the recorded spectra. This structure is only obtained in the spectra calculated with the polarization vector parallel to the incidence plane. When studying the spectra calculated for the two different polarization directions the observation is made that at angles larger than 15° the spectra shown in Fig. 4 actually are dominated by the contribution from the parallel polarization component. This was not the case along the ⟨011⟩ azimuth where the dispersing structure in the calculated spectra actually originated from the perpendicular polarization component. This may possibly explain why the agreement between calculated and experimental results is less satisfactory along the ⟨010⟩ azimuth than along the ⟨011⟩ azimuth.

IV. SUMMARY

The results of a *k*-space-resolved inverse-photoemission investigation of the empty electronic states along the ⟨010⟩ and ⟨011⟩ azimuthal directions from the (100) surfaces of ZrC and VC have been presented. The experimental results have been compared to theoretical spectra calculated using an extended version of the time reversed LEED scheme. At normal incidence angle, i.e., probing states along the Δ direction, only final states of Δ_5 symmetry were observed experimentally, although also transitions to Δ_1 states were predicted in the calculation. We have no explanation as to why these latter structures do not appear in the experimental spectra, but can just note that this has been observed earlier on TiC.[16] Apart from this, the calculated spectra have been shown to reproduce the relative intensities and the trends in the peak dispersions of the experimental spectra fairly well. There was one exception though, the ⟨010⟩ azimuth on VC(100), where the agreement between calculated and recorded spectra was less satisfactory at larger incidence angles.

ACKNOWLEDGMENT

The authors would like to thank the Swedish Natural Science Research Council for their financial support.

[1]P. A. P. Lindberg, P. L. Wincott, L. I. Johansson, and A. N. Christensen, Phys. Rev. B **36**, 4681 (1987).
[2]P. A. P. Lindberg, P. L. Wincott, and L. I. Johansson, Surf. Sci. **189/190**, 761 (1987).
[3]K. L. Håkansson, L. I. Johansson, P. L. Wincott, and D. S. L. Law, Surf. Sci. **251/252**, 108 (1991).
[4]P. A. P. Lindberg, L. I. Johansson, and A. N. Christensen, Surf. Sci. **192**, 353 (1987).
[5]P. A. P. Lindberg and L. I. Johansson, Surf. Sci. **192**, 366 (1987).
[6]P. A. P. Lindberg and L. I. Johansson, Z. Phys. B **68**, 83 (1987).
[7]K. L. Håkansson, L. I. Johansson, P. L. Wincott, and D. S. L. Law, Surf. Sci. **258**, 389 (1991).
[8]K. L. Håkansson, L. I. Johansson, M. Hammar, and M. Göthelid, Phys. Rev. B **47**, 10 769 (1993).
[9]K. L. Håkansson, H. I. P. Johansson, and L. I. Johansson, Phys. Rev. B (to be published).
[10]V. Dose, Surf. Sci. Rep. **5**, 337 (1985), and references therein.
[11]N. V. Smith, Rep. Prog. Phys. **51**, 1227 (1988).
[12]J. F. L. Hopkinson, J. B. Pendry, and D. J. Titterington, Comput. Phys. Commun. **19**, 69 (1980).
[13]C. G. Larsson, Ph.D. thesis, Chalmers University of Technology, Gothenburg, 1982.
[14]K. L. Håkansson, P. L. Wincott, and L. I. Johansson, Surf. Sci. **236**, 169 (1990).
[15]Lars Ilver (private communication) has shown that the energy resolution of the photon detector is improved when layers of selected alkali halides are deposited on the window and the photoemitter.
[16]L. I. Johansson, K. L. Håkansson, and P. L. Wincott, Surf. Sci. **240**, 163 (1990).